Nanoscale

Accepted Manuscript

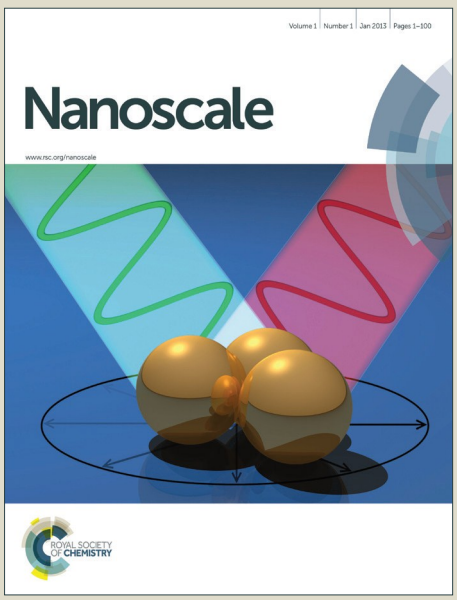

ROYAL SOCIETY OF CHEMISTRY

www.rsc.org/nanoscale

Journal Name

ARTICLE

TiO_2/Vanadates ($Sr_{10}V_6O_{25}$, $Ni_3V_2O_8$, $Zn_2V_2O_7$) Heterostructure Photocatalyst with Enhanced Photocatalytic Activity on Photoreduction of CO_2 into CH_4

Received 00th January 20xx,
Accepted 00th January 20xx

DOI: 10.1039/x0xx00000x

www.rsc.org/

Yabin Yan[a], Yanlong Yu[b], Di Wu[a], Yajun Yang[a] and Yaan Cao[a*]

A series of TiO_2/vanadates ($Sr_{10}V_6O_{25}$, $Ni_3V_2O_8$, $Zn_2V_2O_7$) heterostructure photocatalysts were prepared by a simple sol-gel method. The theory calculation implies the possible energy band match between TiO_2 and vanadates. Characterized by XRD, Raman, TEM, EDX, XPS, absorption spectra, PL and time-resolved PL decay curves, it is revealed that the vanadates, which exist on the surface of TiO_2, could suppress the recombination of charge carriers, prolong the life-time of photogenerated electrons and provide the surface reactive hole sites, improving the photocatalytic activity on photo-reduction of CO_2 into CH_4.

Introduction

In recent years, photoreduction of CO_2 into hydrocarbon fuels has become a new research hotspot for the utilization of renewable energy and the elimination of greenhouse effect. TiO_2 has been widely investigated in this field owing to its good stability and high photocatalytic performance.[1-5] However, due to its large band gap (anatase, 3.2 eV),[6, 7] TiO_2 shows no response to the visible light and the recombination efficiency of photogenerated carriers is relative high, limiting the practical applications.[8, 9] Therefore, it is still of great importance to develop new functional materials with significant photocatalytic performance.

Vanadate photocatalysts have attracted much attention, because of its narrow band gap, stable chemical property and excellent potential of photocatalytic activity.[10,11] Akihiko Kudo et al. reported that the monoclinic $BiVO_4$ showed the outstanding photocatalytic activity for O_2 evolution under visible light irradiation.[12] Yuanyuan Liu et al. reported that the photoreduction of CO_2 in water with $BiVO_4$ led selectively to ethanol.[13] Ping Li et al. reported that $Fe_2V_4O_{13}$ showed great potential for the efficient photoreduction of CO_2 into renewable hydrocarbon fuel.[14] Ryoko Konta et al. prepared Ag_3VO_4 by a solid-state reaction, which was a new visible-light-driven photocatalyst with an ability for O_2 formation.[15]

Therefore, to obtain an enhanced photocatalytic activity on photo-reduction CO_2 into CH_4, we fabricate new heterostructure photocatalyst by adding vanadates into TiO_2 system, which would promote the separation of charge carriers and provide highly reactive hole sites, improving the redox abilities of photocatalyst.

In this work, three different kinds of vanadates ($Sr_{10}V_6O_{25}$, $Ni_3V_2O_8$, $Zn_2V_2O_7$) were composited with TiO_2 to form heterostructure photocatalysts on nanoscale. The band structure of the vanadates is also studied by carrying out the theory calculation. The heterostructures exhibit enhanced photocatalytic activity on photo-reduction CO_2 into CH_4. The influence of vanadates on the structure, behaviors of photogenerated charge carriers and the mechanism of the enhanced photocatalytic activity are also investigated in details.

Experimental

Catalyst Preparation

$Sr_{10}V_6O_{25}$: At room temperature, 10 ml of $Sr(NO_3)_2$ solution (0.3 mol/L) was mixed with 10 ml of Na_3VO_4 solution (0.1 mol/L). After completely mixing, 4 mmol NaOH was added into the solution under vigorous stirring. Half an hour later, the mixture was transferred to 25 ml polytetrafluoroethylene liner. Then the liner was placed into the corresponding high pressure reactor and the whole system was put into the electric constant temperature drying oven at 180 °C for 24 h. After that, the product was washed three times with deionized water and dried at 60 °C. So $Sr_{10}V_6O_{25}$ was obtained.

$Ni_3V_2O_8$ and $Zn_2V_2O_7$: First, 50 ml of $NiCl_2$ solution (0.3 mol/L), NH_4VO_3 solution (0.2 mol/L) and citric acid (1 mol/L) were prepared, respectively. Because NH_4VO_3 was slightly soluble in water, another 10 ml concentrated hydrochloric acid (12 mol/L)

[a] Key Laboratory of Weak-Light Nonlinear Photonics, Ministry of Education, TEDA Applied Physics Institute and School of Physics, Nankai University, Tianjin 300457, China. E-mail: caoya@nankai.edu.cn
[b] College of Material Science & Engineer, Liaoning Technology University, Fuxin 123 000, China

† Footnotes relating to the title and/or authors should appear here.
Electronic Supplementary Information (ESI) available: [details of any supplementary information available should be included here]. See DOI: 10.1039/x0xx00000x

was added into NH_4VO_3 solution for completely dissolution of NH_4VO_3. After mixing the three kinds of the aforesaid solutions, 5 ml ethylene glycol was added in the mixture. Half an hour later, the mixture was heated in water bath at 90 °C for 6 h. Then the product was dried at 140 °C for 12 h. The $Ni_3V_2O_8$ precursor was got. Finally, the sample was triturated to powder and calcined at 700 °C for 2.5 h. So $Ni_3V_2O_8$ powder was completed. $Zn_2V_2O_7$ was prepared using the same protocol, but two points were different. First, $Zn(NO_3)_2$ solution (0.2 mol/L) was used to take the place of $NiCl_2$ solution. Second, the concentrated HCl was replaced with the concentrated HNO_3.

Recombination of TiO_2 and vanadate: At room temperature, 40 mL of anhydrous ethanol was mixed with 1 mL of deionized water. Under vigorous stirring, 12 mL of $Ti(OC_4H_9)_4$ was added into the solution. Then 1 mL of concentrated HCl (12 mol/L) was added to adjust the pH value of the mixture. At 30 min later, a certain mass of vanadate and 1 mL of deionized water was added. The mixture was stirred continuously until the formation of TiO_2 gel. The resultant precipitate was dried at 100 °C for 12 h after aging at room temperature for 24 h and calcined at 450 °C for 2.5 h. Three groups of TiO_2/vanadate photocatalysts were prepared by changing the mass of vanadate added into the mixture. For comparison, pure TiO_2 was synthesized without the addition of vanadate. These samples were respectively designated as pure TiO_2, pure vanadate, TiO_2-vanadate x%, where "x%" represents the nominal mass percentage content of vanadate in the whole sample (vanadate and TiO_2).

Characterization

The XRD patterns were collected on a Rigaku D/max 2500 X-ray diffraction spectrometer (Cu Kα, λ=1.54056 Å). The average crystal size was calculated based on Scherrer equation (D = kλ/Bcosθ). The BET surface areas of the samples were determined by nitrogen adsorption-desorption isotherm measurement at 77 K (Micromeritics Automatic Surface Area Analyzer Gemini 2360, Shimadzu). Raman spectra were taken on a Renishaw in Via Raman microscope by using the785 nm line of Renishaw HPNIR 785 semiconductor laser. The high-resolution transmission electron microscopy (HRTEM) analysis were performed using a Philips Tecnai G2F20 instrument at an accelerating voltage of 200 kV, for which the samples were prepared by applying a drop of ethanol suspension onto an amorphous carbon-coated copper grid and dried naturally. XPS measurements were carried out with an SECA Lab 220i-XL spectrometer by using a monochromated Al-Kα X-ray source (1486.6 eV), and the binding energy was calibrated according to the adventitious C1s peak of 284.8 eV. Diffuse reflectance UV-Visible (UV-Vis) absorption spectra were recorded on a UV-Vis spectrometer (Perkin Elmer Lambda 750，America). The photoluminescence (PL) spectra were measured by fluorescence spectrophotometer (FL3-2-IHR221-NIR-TCSPC, France) using the 340 nm line of a nanosecond Nd:YAG laser (NL303G) as the excitation source. The time-resolved fluorescence decay spectra were measured on iHR320 (HORIBA Jobin Yvon, France) by using the light source of nanoLED. The experimental setup consists of a gas chromatograph (GC7890F, Shanghai Techcomp Instrument Co., Ltd.), a hydrogen generator (SPH-300A, Beijing BCHP Analytical Technology Institute), an automatic air source (SPB-3, Beijing BCHP Analytical Technology Institute) and a computer for data processing. All the measurements were carried out at room temperature (25±2) °C unless stated otherwise.

Evaluation of Photocatalytic Activity

The photoreduction of CO_2 into CH_4 was carried out in a 500 mL quartz tube reactor with 100 mg of catalysts tiled on a glass sheet (3cm×2.5cm) under the ultraviolet light irradiation. A 500 W spherical xenon lamp (Philips, Belgium) was used as the light source. The quartz reactor was located at 10 cm away from the light source and remained vertical to the light beam. The glass sheet with the catalysts was put into the reactor, making it on the underface of the light source. The reactor was continuously inflated by CO_2 gas (99.999%) at a flux of 10 mL min^{-1} for at least 1h, which was enough to ensure that the reactor was utterly full of CO_2 gas. Then 2 ml deionized water was injected into the reactor and the light source was turned on. Every 2 h, the produced concentration of CH_4 and CO was measured by a gas chromatograph (GC7890F, Shanghai Techcomp Instrument Co., Ltd.). Each photocatalytic reduction experiment was repeated three times to evaluate the reproducibility of the results. The blank experiment was tested under identical conditions without catalyst. The chemical reagents were all of analytical grade in the experiments and water was deionized water (>18.2 MΩ cm).

Calculation

The calculations were carried out by a first-principle calculation software package CASTEP. Generalized gradient approximation (GGA)[16, 17] based density-functional theory (DFT) was used to calculate the electronic band structure and density of states (DOS) for pure TiO_2, $Sr_{10}V_6O_{25}$, $Ni_3V_2O_8$ and $Zn_2V_2O_7$, respectively. The pseudopotential used is Vanderbilt-type ultrasoft pseudopotential with $2s^22p^4$, $3s^23p^63d^24s^2$, $5s^2$, $3d^84s^2$, $3d^{10}4s^2$ and $3d^34s^2$ as the valence-electron configurations for the oxygen, titanium, strontium, nickel, zinc and vanadium atoms, respectively. The plane wave energy cutoffs were taken to be 380 eV. In all the cases, geometry optimizations were carried out first, and convergence was assumed when the forces on atoms were less than 50 meV/Å. Compared with experimental results, theoretical calculation usually results in a underestimated band gap, caused by the shortcoming of the exchange-correction functional in describing the excited states.[18, 19] It should be noted that due to the magnetism of nickel ion, Spin polarization was added when the band structure and density of state of $Ni_3V_2O_8$ was calculated.

Results and discussion

Theoretical Calculation

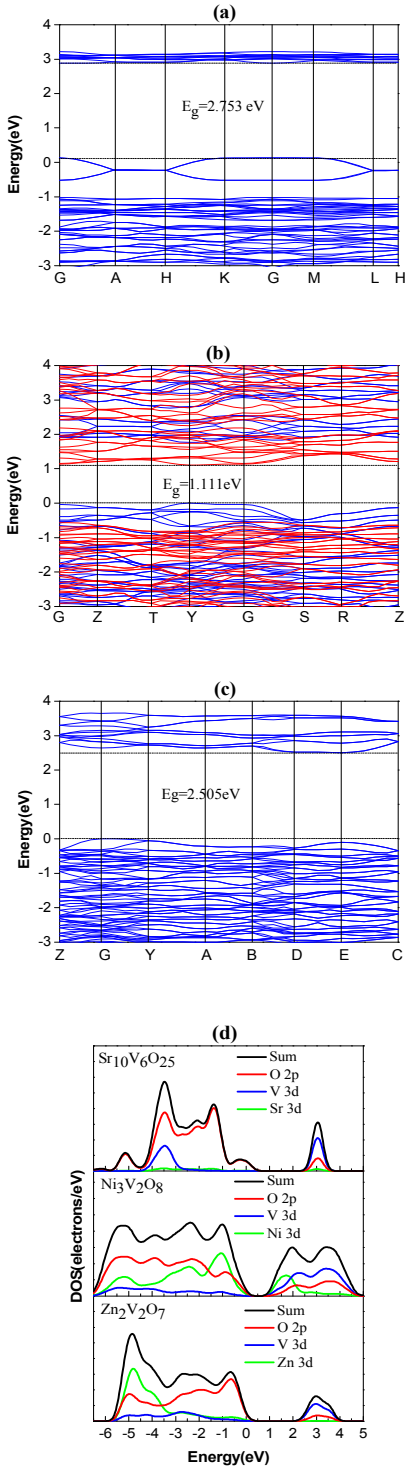

Figure 1. Theoretical calculated band structure for $Sr_{10}V_6O_{25}$ (a), $Ni_3V_2O_8$ (b) and $Zn_2V_2O_7$ (c); (d) Projected density of states (PDOS) for $Sr_{10}V_6O_{25}$, $Ni_3V_2O_8$ and $Zn_2V_2O_7$.

To get the physical insight of the band structure for TiO_2/vanadate composite photocatalyst, the models of pure $Sr_{10}V_6O_{25}$, $Ni_3V_2O_8$, $Zn_2V_2O_7$ and TiO_2 are built and DFT calculation was performed, which are shown in Figure 1 and Figure S1. The zero energy level locates at the maximum of the valence band, corresponding to highest state level that electrons occupy. It is found that the $Sr_{10}V_6O_{25}$ and $Ni_3V_2O_8$ are direct transition materials and $Zn_2V_2O_7$ is an indirect transition material, whose band gaps are 2.753 eV, 1.111eV and 2.505eV, respectively. The calculation result of pure TiO_2 indicates an indirect band gap of 2.644 eV, shown in Figure S1. It is easily observed that, for $Sr_{10}V_6O_{25}$ samples (Figure 1d), the valence band is dominated by O 2p orbitals, hybridized with a small fraction of Sr 3d and V 3d. The conduction band is predominantly V 3d orbitals, hybridized with small amount of O 2p and Sr 3d. For $Ni_3V_2O_8$ samples (Figure 1d), the valence band consist of mainly Ni 3d and O 2p orbitals and the conduction band is dominated by the V 3d orbitals. For $Zn_2V_2O_7$ (Figure 1d), the valence band consist of Zn 3d and O 2p orbitals and the conduction band is composed of V 3d and O 2p orbitals.

According to the discussion above, the addition of vanadates ($Sr_{10}V_6O_{25}$, $Ni_3V_2O_8$, $Zn_2V_2O_7$) into TiO_2 system may extend the absorption into visible region, suppress the recombination of charge carriers and enhance the photocatalytic activity.

Structure of photocatalysts

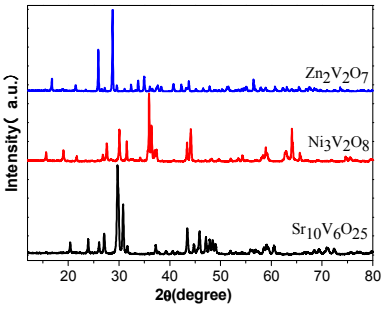

Figure 2. XRD patterns of pure $Sr_{10}V_6O_{25}$, $Ni_3V_2O_8$ and $Zn_2V_2O_7$ samples.

To investigate the crystal structure of the vanadates, XRD patterns of $Sr_{10}V_6O_{25}$, $Ni_3V_2O_8$ and $Zn_2V_2O_7$ is shown in Figure 2. It can be found that the XRD peaks of $Sr_{10}V_6O_{25}$ is completely in accord with the hexagonal phase of (JCPDS 00-052-1578), the characteristic peaks of $Ni_3V_2O_8$ is orthorhombic phase (JCPDS 04-008-9837) and the crystalline phase of $Zn_2V_2O_7$ is the monoclinic phase (JCPDS 04-005-5790). In addition, the XRD patterns of TiO_2-$Sr_{10}V_6O_{25}$ 0.5%, TiO_2-$Ni_3V_2O_8$ 0.5% and TiO_2-$Zn_2V_2O_7$ 0.5% is shown in Figure S2, All four samples exhibit typical anatase structure, no characteristic diffraction peak related to $Sr_{10}V_6O_{25}$, $Ni_3V_2O_8$ and $Zn_2V_2O_7$, is observed, as only a small amount of vanadate is added and its dispersion is high[20]. The lattice parameters, cell volumes and crystal sizes are evaluated and summerized in Table S1. Compared with pure TiO_2, the lattice parameters and cell volumes of TiO_2-$Sr_{10}V_6O_{25}$ 0.5%, TiO_2-$Ni_3V_2O_8$ 0.5% and TiO_2-$Zn_2V_2O_7$ 0.5% remain unchanged, indicating no foreign ions (such as Sr, Zn, Ni and V) are doped into TiO_2 lattice. Moreover, the crystallite sizes of the

compound catalysts decrease and specific surface area (BET) increases, suggesting the addition of vanadate could suppress the grain growth of TiO_2 by providing dissimilar boundary.[21] TiO_2 samples composited with different amount of vanadate are also investigated by XRD, shown in Figure S3, S4 and S5, respectively.

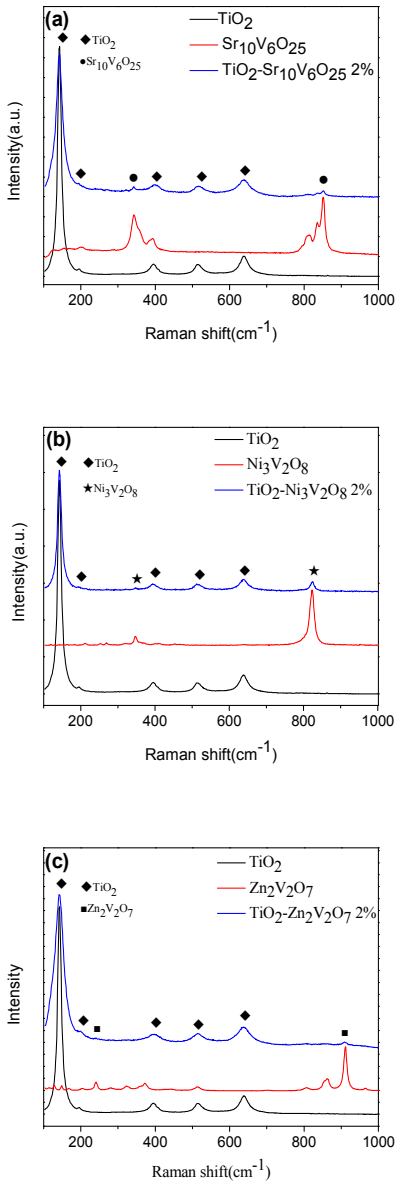

Figure 3. Raman spectra of TiO_2, vanadate and TiO_2-vanadates heterostructure photocatalysts.

Figure 3 shows Raman spectra of pure TiO_2, vanadate and TiO_2-vanadates heterostructure photocatalysts. For pure TiO_2, the typical anatase peaks at about 144 cm^{-1} (Eg), 194 cm^{-1} (Eg), 396 cm^{-1} (B1g), 516 cm^{-1} (A1g and B1g), and 638 cm^{-1} (Eg) are observed, respectively.[22,23] It is easily seen that the TiO_2-vanadate samples still remain anatase structure. In addition, compared with TiO_2, two peaks at about 338 cm^{-1} and 845 cm^{-1} is ascribed to pure $Sr_{10}V_6O_{25}$ in TiO_2-$Sr_{10}V_6O_{25}$ 2% (Figure 3a). In Figure 3b, two apparent peaks at about 343 cm^{-1} and 819 cm^{-1} for the TiO_2-$Ni_3V_2O_8$ 2% sample are also observed, confirming the presence of $Ni_3V_2O_8$ in the composite. For TiO_2-$Zn_2V_2O_7$ 2% sample (Figure 3c), the peaks well matched with $Zn_2V_2O_7$ locate at 235 cm^{-1} and 906 cm^{-1}. The above results indicate an existence of vanadates in the composites.

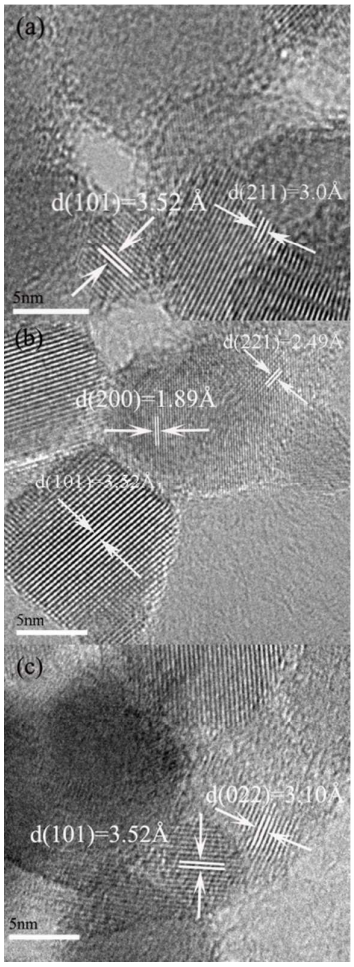

Figure 4. HRTEM images of (a) TiO_2-$Sr_{10}V_6O_{25}$ 2.0%, (b) TiO_2-$Ni_3V_2O_8$ 2.0% and (c) TiO_2-$Zn_2V_2O_7$ 2.0% samples.

For confirm the existence of $Sr_{10}V_6O_{25}$, $Ni_3V_2O_8$ and $Zn_2V_2O_7$, TEM and HRTEM of TiO_2-$Sr_{10}V_6O_{25}$ 2.0%, TiO_2-$Ni_3V_2O_8$ 2.0% and TiO_2-$Zn_2V_2O_7$ 2.0% are shown in Figure 4. A clear fringe spacing (d) of 3.52 Å is observed for TiO_2-$Sr_{10}V_6O_{25}$ 2.0% (Figure 4a), TiO_2-$Ni_3V_2O_8$ 2.0% (Figure 4b) and TiO_2-$Zn_2V_2O_7$ 2.0% (Figure 4c), suggesting the existence of TiO_2 anatase structure. The fringe spacing (d) of 1.89 Å in Figure 3a is ascribed to the (200) plane of TiO_2. Moreover, three different fringe spacing (d) of 3.00 Å, 2.49 Å and 3.10 Å is found in Figure 4a, 4b and 4c, attributed to the (211) plane of $Sr_{10}V_6O_{25}$, (221) planes of $Ni_3V_2O_8$ and (022) planes of $Zn_2V_2O_7$, respectively. Incidentally, the TiO_2-vanadate heterostructure photocatalysts are further confirmed by EDX spectrum, as shown in Figure S6. For TiO_2-$Sr_{10}V_6O_{25}$ 2.0% (Figure S6a), the major elements are the Ti, O, Sr and V. In Figure S6b, it is easily to determine the Ti, O, Ni and V as major elements for TiO_2-

$Ni_3V_2O_8$ 2.0%. In Figure S6c, it appears clearly that the TiO_2-$Zn_2V_2O_7$ 2.0% is primarily constituted of Ti, O, Zn and V elements. These discussions imply all three groups of TiO_2-vanadate photocatalysts behave as a well-crystallized heterostructure on nanoscale between TiO_2 and vanadate nanoparticle.

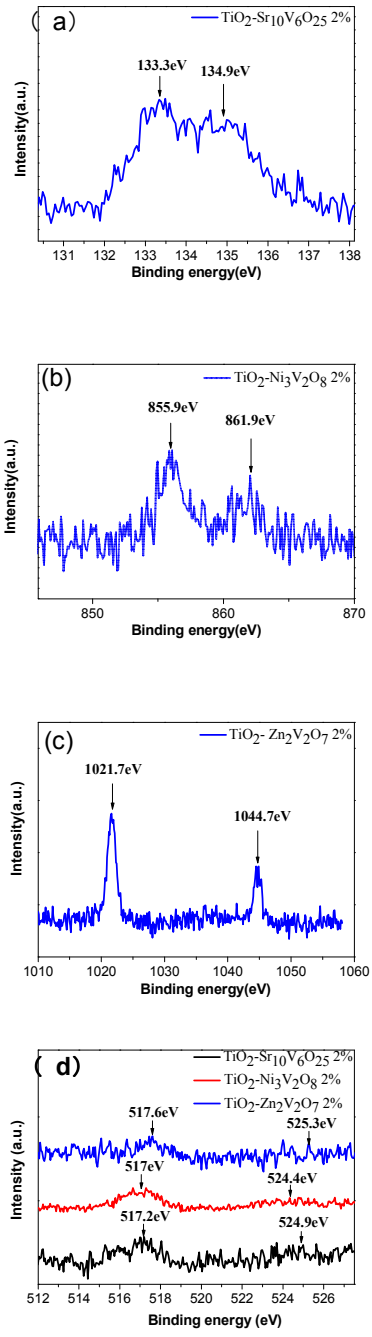

Figure 5. Sr 3d (a) XPS spectra of TiO_2-$Sr_{10}V_6O_{25}$ 2%; Ni 2p (b) XPS spectra of TiO_2-$Ni_3V_2O_8$ 2%; Zn 2p (c) XPS spectra of TiO_2-$Zn_2V_2O_7$ 2%; V2p (d) XPS spectras of TiO_2-$Sr_{10}V_6O_{25}$ 2%, TiO_2-$Ni_3V_2O_8$ 2% and TiO_2-$Zn_2V_2O_7$ 2%.

XPS analysis is performed to investigate the existing states of $Sr_{10}V_6O_{25}$, $Ni_3V_2O_8$ and $Zn_2V_2O_7$ in TiO_2-$Sr_{10}V_6O_{25}$ 2.0%, TiO_2-$Ni_3V_2O_8$ 2% and TiO_2-$Zn_2V_2O_7$ 2%, respectively. For TiO_2-$Sr_{10}V_6O_{25}$ 2% sample, the double peaks attributed to Sr $3d_{5/2}$ and Sr $3d_{3/2}$ are at about 133.3 and 134.9 eV in the Sr 3d spectra (Figure 5a) and the V $2p_{3/2}$ and V $2p_{1/2}$ peaks (Figure 5d)are around 517.2 and 524.9eV, which are the same as that for pure $Sr_{10}V_6O_{25}$, shown in Figure S7. In Figure 5b and 5d, the binding energy of Ni $2p_{3/2}$ and Ni $2p_{1/2}$ are around 855.9 and 861.9 eV, and V $2p_{3/2}$ and V $2p_{1/2}$ is at about 517.0 and 524.4 eV, which could be ascribed to that of $Ni_3V_2O_8$,[24] shown in Figure S8. As shown in Figure 5c and 5d, the Zn 2p (1021.7 and 1044.7eV) and V 2p (517.6 and 525.3 eV) are ascribed to that for $Zn_2V_2O_7$, as shown in Figure S9. The XPS results of TiO_2 coupled with different amount of vanadate is presented in Figure S7, S8 and S9. These XPS results further demonstrate the existence of vanadate in the photocatalysts, which agree with the Raman andTEM results.

Band Structure of the Photocatalysts

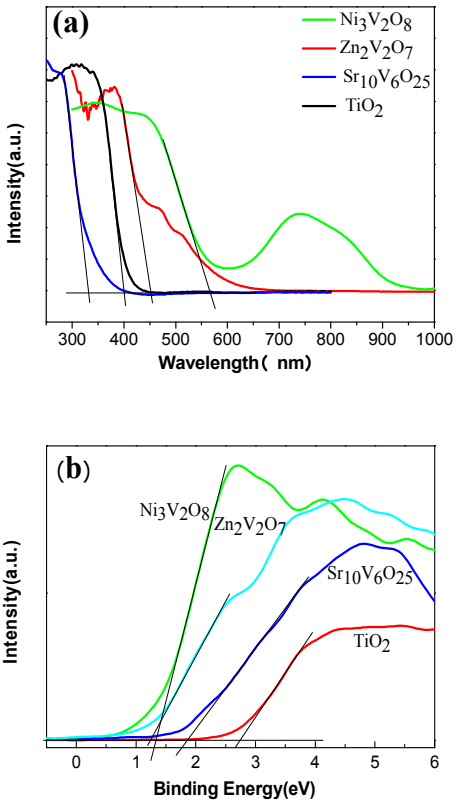

Figure 6. (a) Diffuse reflectance UV-Vis spectra of TiO_2, $Sr_{10}V_6O_{25}$, $Ni_3V_2O_8$ and $Zn_2V_2O_7$; (b) XPS valence band spectra of TiO_2, $Sr_{10}V_6O_{25}$, $Ni_3V_2O_8$ and $Zn_2V_2O_7$.

Diffuse reflectance UV–vis absorption spectra and XPS valence band (VB) spectra are plotted in Figure 6 to investigate the band structure of the heterostructured photocatalyst. Figure 6a shows the diffuse reflectance UV–vis absorption spectra for pure TiO_2, $Sr_{10}V_6O_{25}$, $Ni_3V_2O_8$ and $Zn_2V_2O_7$ samples. The strong absorption in

UV region for all four photocatalysts is ascribed to the band to band transition. The absorption onset edge for TiO_2 is 399.8 nm, corresponding to a band gap of 3.10 eV.[25] The band gaps of $Sr_{10}V_6O_{25}$, $Ni_3V_2O_8$ and $Zn_2V_2O_7$ is about 3.73, 2.19 and 2.75eV, respectively, because their absorption onset edges locate at 332.3, 566.0 and 451.2 nm, respectively. In addition, the absorption peak at 500 nm for $Zn_2V_2O_7$ and 750nm for $Ni_3V_2O_8$ is ascribed to transition from valence band to the energy level of oxygen vacancies. The XPS valence band spectra of TiO_2, $Sr_{10}V_6O_{25}$, $Ni_3V_2O_8$ and $Zn_2V_2O_7$ are shown in Figure 6b. The energy level is in alignment with the work function of the XPS instrument (4.10 eV, Fermi level). The binding energy of the onset edge for the O2p peak reveals the energy gap between the Fermi level and valence band maximum.[6] In Figure 6b, the onset edge of binding energy (the valence band) of TiO_2, $Sr_{10}V_6O_{25}$, $Ni_3V_2O_8$ and $Zn_2V_2O_7$ are 2.80, 1.87, 1.34 and 1.28eV(2.40, 1.47, 0.94 and 0.88 V ; vs NHE), respectively. According to the band gaps of TiO_2, $Sr_{10}V_6O_{25}$, $Ni_3V_2O_8$ and $Zn_2V_2O_7$ (3.10, 3.73, 2.19 and 2.75eV), the conduction band for TiO_2, $Sr_{10}V_6O_{25}$, $Ni_3V_2O_8$ and $Zn_2V_2O_7$ is at -0.70, -2.26, -1.25 and -1.87 V (vs NHE), respectively. Moreover, the energy levels of the oxygen vacancies for $Zn_2V_2O_7$ and $Ni_3V_2O_8$ are locate at about 0.27 and 0.54 eV below the conduction band, respectively. Therefore, the band structure of TiO_2/vanadate photocatalysts could be drawn in Figure 9.

As shown in Figure S10d, after the addition of vanadates, the absorption in visible region is enhanced significantly and extended from UV region to infrared region (400~800nm) for TiO_2-$Sr_{10}V_6O_{25}$ 0.5%, TiO_2-$Ni_3V_2O_8$ 0.5% and TiO_2-$Zn_2V_2O_7$ 0.5%. These results imply that the addition of vanadates is in favor of the enhancement of photocatalytic activity on reduction of CO_2 into CH_4. The absorption spectra of TiO_2 coupled with different amount of vanadates are plotted in Figure S10.

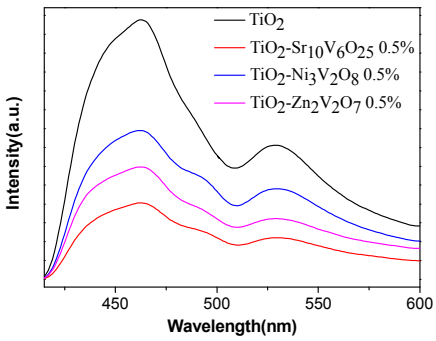

Figure 7. Photoluminescence spectra of pure TiO_2, TiO_2-$Sr_{10}V_6O_{25}$ 0.5%, TiO_2-$Ni_3V_2O_8$ 0.5% and TiO_2-$Zn_2V_2O_7$ 0.5% samples.

To investigate the behaviors of photogenerated charge carriers for photocatalysts, Photoluminescence spectra (PL) of TiO_2, TiO_2-$Sr_{10}V_6O_{25}$ 0.5%, TiO_2-$Ni_3V_2O_8$ 0.5% and TiO_2-$Zn_2V_2O_7$ 0.5% are shown in Figure 7. Two peaks located at 464 and 529 nm are observed for all photocatalysts, which are ascribed to the transition from the oxygen vacancies with two trapped electrons and one trapped electron to the valence band of TiO_2, respectively.[26-30] The energy levels of the oxygen vacancies are evaluated to be 0.43 and 0.76 eV below the conduction band of TiO_2, respectively. The photogenerated electrons in conduction band fall into the energy levels of the oxygen vacancies via a nonirradiative process, then recombine with the photogenerated holes in valence band, accompanying with a fluorescent emission.[31] Hence, a decrease of PL emission usually implies the inhibited recombination of photogenerated charge carriers. Compared with pure TiO_2, the PL spectra of TiO_2-$Sr_{10}V_6O_{25}$ 0.5%, TiO_2-$Ni_3V_2O_8$ 0.5% and TiO_2-$Zn_2V_2O_7$ 0.5% is weakened, suggesting the addition of vanadate can suppress the recombination of the photogenerated carriers effectively.

Table 1. Fluorescence Lifetimes of pure TiO_2, TiO_2-$Zn_2V_2O_7$ 0.5%, TiO_2-$Ni_3V_2O_8$ 0.5% and TiO_2-$Sr_{10}V_6O_{25}$ 0.5%.

	TiO_2	TiO_2-$Zn_2V_2O_7$ 0.5%	TiO_2-$Ni_3V_2O_8$ 0.5%	TiO_2-$Sr_{10}V_6O_{25}$ 0.5%
τ_1 (ns)	0.05	0.07	0.11	0.10
τ_2 (ns)	12.88	14.46	14.55	16.67

To further investigate the behaviors of the photogenerated carriers, the time-resolved PL decay curves of TiO_2, TiO_2-$Zn_2V_2O_7$ 0.5%, TiO_2-$Ni_3V_2O_8$ 0.5% and TiO_2-$Sr_{10}V_6O_{25}$ 0.5% are shown in Figure S11. As shown in Table 1, the τ_1 and τ_2 values for four samples were calculated via double exponential decay fitting.[32] For metal oxide, the PL decay curve arises from a combination of a nonradiative (τ_1) process and a radiative (τ_2) process.[33-35] The fast decay process (τ_1) is usually attributed to the nonradiative relaxation process relevant to defects of oxide, and the slow decay range (τ_2) comes from the radiative process which is related to the recombination of photogenerated holes and electrons.[31] From Table 1, it is clear that the τ_2 for pure TiO_2 is 12.88 ns. After modification with vanadate, τ_2 values of TiO_2-$Zn_2V_2O_7$ 0.5%, TiO_2-$Ni_3V_2O_8$ 0.5% and TiO_2-$Sr_{10}V_6O_{25}$ 0.5% are prolonged to 14.46, 14.55 and 16.67 ns, respectively, which is longer than that for pure TiO_2, implying efficient separation of photogenerated carriers. These results indicate the addition of vanadates can promote the separation of photogenerated charge carriers effectively, leading to an enhanced photocatalytic activity for TiO_2-vanadates photocatalyst.

Photocatalytic activity

Photocatalytic activity of the catalyst is evaluated by photo-reduction of CO_2 and H_2O into CH_4 under UV light irradiation. CO is the intermediate product and CH_4 is the final product. The photocatalytic results of pure TiO_2, TiO_2-$Sr_{10}V_6O_{25}$ 0.5%, TiO_2-$Ni_3V_2O_8$ 0.5% and TiO_2-$Zn_2V_2O_7$ 0.5% samples are shown in Figure 8 and Table S2. It is observed that seldom CH_4 is detected (0.399 μmol) in blank experiment. About 0.409 μmol of CH_4 is generated in the presence of pure TiO_2 after 8 hours' irradiation. The photocatalytic activity for pure vanadates is also tested, shown in Figure S12a. The generated amount of CH_4 for $Sr_{10}V_6O_{25}$, $Ni_3V_2O_8$ and $Zn_2V_2O_7$ is about 0.549, 0.4, 0.563μmol, respectively. Moreover, the photocatalytic experiment of TiO_2 coupled with different

amount of vanadates (TiO_2-$Sr_{10}V_6O_{25}$ x%, TiO_2-$Ni_3V_2O_8$ x% and TiO_2-$Zn_2V_2O_7$ x%) are performed and TiO_2-$Sr_{10}V_6O_{25}$ 0.5%, TiO_2-$Ni_3V_2O_8$ 0.5% and TiO_2-$Zn_2V_2O_7$ 0.5% exhibit the best photocatalytic activity in each group of the TiO_2-vanadate photocatalysts (FigureS13a, S14a and S15a). Compared with pure TiO_2, the photocatalytic activity of TiO_2-$Sr_{10}V_6O_{25}$ 0.5%, TiO_2-$Ni_3V_2O_8$ 0.5% and TiO_2-$Zn_2V_2O_7$ 0.5% is enhanced and 3.369, 2.184, 1.972 μmol of CH_4 is generated, respectively. Among these samples, the photocatalytic activity of TiO_2-$Ni_3V_2O_8$ 0.5% and TiO_2-$Zn_2V_2O_7$ 0.5% (CH_4 generation amount (mol) and specific photocatalytic activity ($mol \cdot g^{-1} \cdot h^{-1}$) is about 5.3 and 4.8 times higher than that of pure TiO_2, respectively. TiO_2-$Sr_{10}V_6O_{25}$ 0.5% exhibits the best photocatalytic performance whose CH_4 generation amount (mol) and specific photocatalytic activity is 8.3 times as that of pure TiO_2. The amount of generated CO is also detected, shown in Figure 8b, S12b, S13b, S14b and S15b. These results suggest that the addition of vanadate ($Sr_{10}V_6O_{25}$, $Ni_3V_2O_8$ and $Zn_2V_2O_7$) is an effective method to improve the photocatalytic activity on reduction of CO_2 into CH_4 for TiO_2 based photocatalyst.

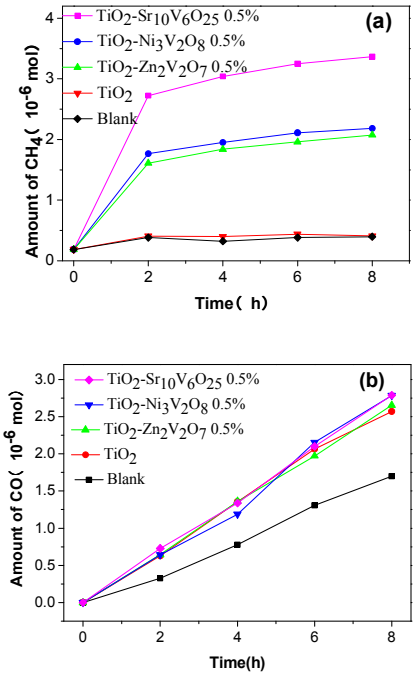

Figure 8. Photocatalytic activity for reduction of CO_2 into CH_4 (a) and CO (b) of pure TiO_2, TiO_2-$Sr_{10}V_6O_{25}$ 0.5%, TiO_2-$Ni_3V_2O_8$ 0.5% and TiO_2-$Zn_2V_2O_7$ 0.5% under UV light irradiation for 8 h.

Photocatalytic mechanism

The mechanism of photocatalytic reduction of CO_2 into CH_4 is shown in equation (1)-(3).[36-38] The photogenerated electrons and holes are excited under irradiation (hv) (1); The photogenerated holes in the valence band are captured by water molecules absorbed on the surface of the catalyst, producing hydroxyl radicals (•OH) and hydrogen ions (H^+). Then the water molecules further oxidized by h^+ and •OH for formation of O_2 and H^+ (2), (0.82 V, vs NHE); The photogenerated electrons on the conduction band react with CO_2 absorbed on the surface of catalyst, resulting in the production of CO (the intermediate product) and O_2. Meanwhile, the carbon radicals (•C) are formed through CO and e^-. Finally, •C react with H^+ and e^- to generate CH_4 (3)(-0.24V ,vs NHE).

catalyst + hv → e^- + h^+ (1)

$H_2O + h^+ \rightarrow \bullet OH + H^+$

$\bullet OH + H_2O + 3h^+ \rightarrow O_2 + 3H^+$

$2H_2O + 4h^+ \rightarrow O_2 + 4H^+$ E^o_{redox} = 0.82 V vs NHE (2)

$2CO_2 + 4e^- \rightarrow 2CO + O_2$ E^o_{redox} = -0.12V vs NHE

$2CO + 4e^- \rightarrow 2\bullet C + O_2$

$\bullet C + 4e^- + 4H^+ \rightarrow CH_4$ E^o_{redox} = 0.13V vs NHE

$CO_2 + 8e^- + 8H^+ \rightarrow CH_4 + 2H_2O$ E^o_{redox} = -0.24 V vs NHE (3)

The potential of the valence band for TiO_2 (2.40 V, vs NHE) is more positive than E^o_{redox} (H_2O/H^+, 0.82 V, vs NHE). And the potential of the conduction band for TiO_2 (-0.70 V, vs NHE), is more negative than E^o_{redox} (CO_2/CH_4, -0.24 V, vs NHE). So the photogenerated electrons and holes for TiO_2 could take part in the photo-reduction of CO_2 into CH_4 in photocatalytic process. However, the photocatalytic activity of TiO_2 is limited due to its large band gap (anatase, 3.2 eV) and high recombination rate of the photogenerated charge carriers.

The energy band structure of TiO_2/vanadate heterostructure is shown in Figure 9. The potential of the conduction band of TiO_2 (-0.70 V， vs NHE) is more negative than E^o_{redox} (CO_2/CH_4, -0.24 V, vs NHE), and the valence band of vanadates ($Sr_{10}V_6O_{25}$, 1.47 V; $Ni_2V_2O_7$, 0.94V; $Zn_2V_2O_7$, 0.88V vs NHE) are all more positive than E^o_{redox} (H_2O/H^+, 0.82 V, vs NHE), suggesting the possibility for the photo reduction of CO_2 into CH_4 in photocatalytic process. Moreover, compared with pure TiO_2, the absorption in visible light region is enhanced significantly and extended from UV to visible region (400~800nm), increasing the amount of photogenerated charge carriers effectively for TiO_2/vanadate photocatalyst. Meanwhile, the photogenerated electrons in the conduction band of vanadates would transfer to that of TiO_2; the photogenerated holes on the valence band of TiO_2 would migrate to that of vanadate. Hence, the photoinduced electrons and holes are separated effectively at the interface between TiO_2 and vanadate nanoparticle. Moreover, the lifetime of photogenerated electrons is also prolonged in comparison with TiO_2, owing to the formation of heterostructure on nanoscale for TiO_2/vanadate. In addition, because of the vanadate particles at the interface, the photogenerated hole reactive sites promote the holes to participate the photocatalytic reaction. Therefore, the photogenerated electrons and holes could participate in the photo-reduction of CO_2 into CH_4 efficiently, resulting in an enhanced photocatalytic activity compared with pure TiO_2.

For the TiO_2/vanadate photocatalysts, the photogenerated electrons of catalysts possess the same reduction ability, as the electrons transfer to the conduction band of TiO_2 for all samples. Furthermore, the potential of the valence band for $Zn_2V_2O_7$ is almost the same as that of $Ni_3V_2O_8$, implying similar oxidation abilities of the photogenerated holes and photocatalytic activity for the TiO_2-$Zn_2V_2O_7$ 0.5% and TiO_2-$Ni_3V_2O_8$ 0.5% photocatalysts. In comparison with TiO_2-$Zn_2V_2O_7$ 0.5% and TiO_2-$Ni_3V_2O_8$ 0.5%, the photogenerated charge carriers of TiO_2-$Sr_{10}V_6O_{25}$ 0.5% are separated more efficiently and the lifetime of photogenerated electrons are also prolonged. This indicates that more photogenerated electrons and holes could take part in the

photocatalytic activity for TiO_2-$Sr_{10}V_6O_{25}$ 0.5% sample, resulting in a better photocatalytic activity than TiO_2-$Zn_2V_2O_7$ 0.5% and TiO_2-$Ni_3V_2O_8$ 0.5%.

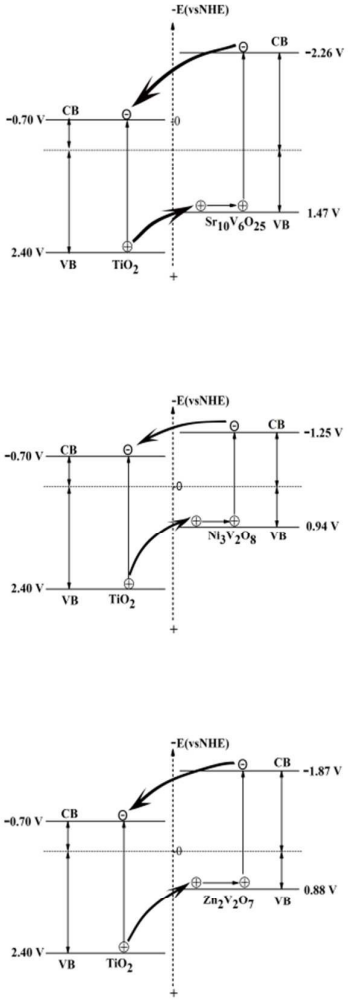

Figure 9. Schematic band structure of TiO_2/vanadate composite photocatalysts.

Conclusions

A series of heterostructure photocatalyst TiO_2 / vanadates ($Sr_{10}V_6O_{25}$, $Ni_3V_2O_8$ and $Zn_2V_2O_7$), were prepared and exhibit improved photocatalytic activity on photo-reduction of CO_2 into CH_4, compared with pure TiO_2. The band structure and DOS of three vanadates are investigated in details. The addition of vanadates ($Sr_{10}V_6O_{25}$, $Ni_3V_2O_8$ and $Zn_2V_2O_7$) could promote the separation of photogenerated charge carriers, prolong the lifetime of photogenerated electrons and provide the hole reactive sites on the surface, indicating more photogenerated charge carriers could take part in the photocatalytic reaction efficiently, improving the photocatalytic activity. This work may offer a new strategy to fabricate and design new photocatalyst with high photocatalytic performance, which can be applied in many fields.

Acknowledgements

This work was supported by the National Natural Science Foundation of China (Nos, 21173121 and 51372120).

Notes and references

1 Inoue, T.; Fujishima, A.; Konishi, S.; Honda, K. Photoelectrocatalytic reduction of carbon dioxide in aqueous suspensions of semiconductor powders. Nature 1979, 277, 637-638.

2 Pankaj Pathak; Mohammed J. Meziani; Yin Li; LaShonda T. Cureton; Ya-Ping Sun. Improving photoreduction of CO_2 with homogeneously dispersed nanoscale TiO_2 catalysts. Chem. Commun., 2004, 1234–1235.

3 Khan, S. U.; Al-Shahry, M.; Ingler, W. B. Efficient Photochemical Water Splitting by a Chemically Modified N-TiO_2. Science 2002, 297, 2243−2245.

4 Hagfeldt, A.; Graetzel, M. Light-Induced Redox Reactions in Nanocrystalline Systems. Chem. Rev. 1995, 95, 49−68.

5 Lianjun Liu; Huilei Zhao; Jean M. Andino; Ying Li. Photocatalytic CO_2 Reduction with H_2O on TiO_2 Nanocrystals: Comparison of Anatase, Rutile, and Brookite Polymorphs and Exploration of Surface Chemistry. ACS Catal. 2012, 2, 1817−1828.

6 Cao, Y.; He, T.; Chen, Y.; Cao, Y. Fabrication of Rutile TiO_2−Sn/Anatase TiO_2−N Heterostructure and Its Application in Visible-Light Photocatalysis. J. Phys. Chem. C 2010, 114, 3627−3633.

7 Wang, E.; He, T.; Zhao, L.; Chen, Y.; Cao, Y. Improved Visible Light Photocatalytic Activity of Titania Doped with Tin and Nitrogen. J. Mater. Chem. 2010, 21, 144−150.

8 Ding, Z.; Lu, G. Q.; Greenfield, P. F. Role of the Crystallite Phase of TiO_2 in Heterogeneous Photocatalysis for Phenol Oxidation in Water. J. Phys. Chem. B 2000, 104, 4815-4820.

9 Horst Kisch; Ling Zang; Christian Lange; Wilhelm F. Maier; Christina Antonius; Dieter Meissner. Modified, Amorphous Titania-A Hybrid Semiconductor for Detoxification and Current Generation by Visible Light. Angew. Chem. Int. Ed. 1998, 37, 3034-3036.

10 J. Ye ; Z. Zou; H. Arakaw; M. Oshikiri ; M. Shimoda ; A. Matsushita; T. Shishido. Correlation of crystal and electronic structures with photophysical properties of water splitting photocatalysts $InMO_4$ (M = V^{5+}, Nb^{5+}, Ta^{5+}). J. Photochem Photobiol A 2002, 148, 79-83.

11 H. Harada; C. Hosoki; A. Kudob. Overall water splitting by sonophotocatalytic reaction: the role of powdered photocatalyst and an attempt to decompose water using a visible-light sensitive photocatalyst. J. Photochem Photobiol A 2001, 141, 219-224.

12 Akihiko Kudo; Keiko Omori; Hideki Kato. A Novel Aqueous Process for Preparation of Crystal Form-Controlled and Highly Crystalline $BiVO_4$ Powder from Layered Vanadates at Room Temperature and Its Photocatalytic and Photophysical Properties. J. Am. Chem. Soc. 1999, 121, 11459-11467.

13 Y. Liu; B. Huang; Y. Dai; X. Zhang; X. Qin; M. Jiang; M.- H. Whangbo, Selective Ethanol Formation from Photocatalytic Reduction of Carbon-dioxide in Water with $BiVO_4$ Photocatalyst. Catal. Comm. 2009, 11(3), 210-213.

14 Ping Li; Yong Zhou; Wenguang Tu; Qi Liu; Shicheng Yan; Zhigang Zou. Direct Growth of $Fe_2V_4O_{13}$ Nanoribbons on a Stainless-Steel Mesh for Visible-Light Photoreduction of CO_2 into Renewable Hydrocarbon Fuel and Degradation of Gaseous Isopropyl

Alcohol. Chem Plus Chem. 2013, 78(3), 274–278.
15 Ryoko Konta; Hideki Kato; Hisayoshi Kobayashi; Akihiko Kudo. Photophysical properties and photocatalytic activities under visible light irradiation of silver vanadates. Phys. Chem. Chem. Phys. 2003, 5, 3061−3065.
16 Xiang, Q.; Yu, J.; Jaroniec, M. Nitrogen and Sulfur Co-Doped TiO_2 Nanosheets with Exposed {001} Facets: Synthesis, Characterization and Visible-Light Photocatalytic Activity. Phys.Chem. Chem. Phys. 2011, 13, 4853−4861.
17 Feng, N.; Zheng, A.; Wang, Q.; Ren, P.; Gao, X.; Liu, S.-B.; Shen, Z.; Chen, T.; Deng, F. Boron Environments in B-Doped and (B, N)-Codoped TiO_2 Photocatalysts: a Combined Solid-State NMR and Theoretical Calculation Study. J. Phys. Chem. C 2011, 115, 2709−2719.
18 Yu, J.; Dai, G.; Xiang, Q.; Jaroniec, M. Fabrication and Enhanced Visible-Light Photocatalytic Activity of Carbon Self-Doped TiO_2 Sheets with Exposed {001} Facets. J. Mater. Chem. 2011, 21, 1049−1057.
19 Di Valentin, C.; Pacchioni, G.; Selloni. A. Theory of Carbon Doping of Titanium Dioxide. Chem. Mater. 2005, 17, 6656−6665.
20 YuLin Min, Kan Zhang, YouCun Chen, YuanGuang Zhang. Synthesis of novel visible light responding vanadate/TiO_2 heterostructure photocatalysts for application of organic pollutants. Chemical Engineering Journal 2011, 175, 76– 83.
21 Cao, Y.; He, T.; Zhao, L.; Wang, E.; Yang, W.; Cao, Y. Structure and Phase Transition Behavior of Sn^{4+}-Doped TiO_2 Nanoparticles. J. Phys. Chem. C 2009, 113, 18121−18124.
22 Zhang, W.; He, Y.; Zhang, M.; Yin, Z.; Chen, Q. Raman scattering study on anatase TiO_2 nanocrystals. J. Phys. D: Appl. Phys. 2000, 33 (8), 912.
23 J. Wang, Y. Yu, S. Li, L. Guo, E. Wang, Y. Cao, Doping behavior of Zr^{4+}Ions inZr^{4+}-doped TiO_2nanoparticles, J. Phys. Chem. C 2013,117, 27120–27126.
24 Xu Ai-ju; Zhaorigtu Bao; Jia Mei-lin; Lin Qin. Study on Performance of $Ni_3V_2O_8$ Catalyst and Analysis of X-Ray Photoelectron Spectroscopy. Spectro scopy and Spectr al Analy sis. 2007, 27, 2134-2138.
25 Gao, B.; Ma, Y.; Cao, Y.; Yang, W.; Yao, J. Great Enhancement of Photocatalytic Activity of Nitrogen-Doped Titania by Coupling with Tungsten Oxide. J. Phys. Chem. B 2006, 110, 14391−14397.
26 Enjun Wang; Wensheng Yang; Yaan Cao. Unique Surface Chemical Species on Indium Doped TiO_2 and Their Effect on the Visible Light Photocatalytic Activity. J. Phys. Chem. C 2009, 113, 20912–20917.
27 Di Li; Hajime Haneda; Shunichi Hishita; Naoki Ohashi. Visible-Light-Driven N-F-Codoped TiO_2 Photocatalysts. 2. Optical Characterization, Photocatalysis, and Potential Application to Air Purification. Chem. Mater. 2005, 17, 2596-2602.
28 Serpone, N.; Lawless, D.; Khairutdinov, R. Size Effects on the Photophysical Properties of Colloidal Anatase TiO_2 Particles: Size Quantization or Direct Transitions in This Indirect Semiconductor. J. Phys. Chem. 1995, 99, 16646-16654.
29 Jia-Guo Yu; Huo-Gen Yu; Bei Cheng; Xiu-Jian Zhao; Jimmy C. Yu; Wing-Kei Ho. The Effect of Calcination Temperature on the Surface Microstructure and Photocatalytic Activity of TiO_2 Thin Films Prepared by Liquid Phase Deposition. J. Phys. Chem. B 2003, 107, 13871-13879.
30 Saraf L. V.; Patil S. I.; Ogale S. B.; Sainkar S. R.; Kshirsager S. T. Synthesis of Nanophase TiO_2 by Ion Beam Sputtering and Cold Condensation Technique. Int. J. Mod. Phys. B 1998, 12, 2635-2647.
31 Jixiang Yuan; Qiang Wu; Peng Zhang; Jianghong Yao; Tao He; Yaan Cao. Synthesis of Indium Borate and Its Application in Photodegradation of 4-Chlorophenol. Environ. Sci. Technol. 2012, 46, 2330−2336.
32 Anjun Qin; Cathy K. W. Jim; Youhong Tang; Jacky W. Y. Lam; Jianzhao Liu; Faisal Mahtab; Ping Gao; Benzhong Tang. Aggregation-Enhanced Emissions of Intramolecular Excimers in Disubstituted Polyacetylenes. J. Phys. Chem. B 2008, 112, 9281–9288.
33 Wang, E.; Zhang, P.; Chen, Y.; Liu, Z.; He, T.; Cao, Y. Improved Visible-Light Photocatalytic Activity of Titania Activated by Nitrogen and Indium Modification. J. Mater. Chem. 2012, 22, 14443−14449.
34 Zhong, Y.; Djurisic, A. B.; Hsu, Y. F.; Wong, K. S.; Brauer, G.; Ling, C. C.; Chan, W. K. Exceptionally Long Exciton Photoluminescence Lifetime in ZnO Tetrapods. J. Phys. Chem. C 2008, 112, 16286−16295.
35 Koida, T.; Chichibu, S.; Uedono, A.; Tsukazaki, A.; Kawasaki, M.; Sota, T.; Segawa, Y.; Koinuma, H. Correlation Between the Photoluminescence Lifetime and Defect Density in Bulk and EpitaxialZnO. Appl. Phys. Lett. 2003, 82, 532−534.
36 Oomman K. Varghese; Maggie Paulose; Thomas J. LaTempa and Craig A. Grimes. High-Rate Solar Photocatalytic Conversion of CO_2 and Water Vapor to Hydrocarbon Fuels. Nano Lett. 2009, 9 (2), 731–737.
37 Yasuo Izumi. Recent advances in the photocatalytic conversion of carbon dioxide to fuels with water and/or hydrogen using solar energy and beyond. Coordination Chemistry Reviews 2013, 257, 171–186.
38 Seng Sing Tan; Linda Zou; Eric Hu. Photocatalytic reduction of carbon dioxide into gaseous hydrocarbon using TiO_2 pellets. Catalysis Today 2006, 115, 269–273.